PNAS Nexus, 2023, 2, 1–11
https://doi.org/10.1093/pnasnexus/pgad359
Advance access publication 28 November 2023
Research Report

Carboxyl nanodiamonds inhibit melanoma tumor metastases by blocking cellular motility and invasiveness

Sushreesangita P. Behera [a], Witty Tyagi [b] and Rajiv K. Saxena [a,*]

[a]Faculty of Life Sciences and Biotechnology, South Asian University, New Delhi 110068, India
[b]Molecular Oncology Laboratory, National Institute of Immunology, New Delhi 110067, India
*To whom correspondence should be addressed: Email: rksaxena@sau.int
Edited By: Connie Eaves

Abstract

Carboxyl nanodiamond (cND) nanoparticles are actively internalized by B16F10 melanoma cells in culture. Treatment of B16F10 tumor cells with cNDs in vitro inhibited their ability to (i) migrate and invade through porous membranes in a transwell culture system, (ii) secrete matrix metalloproteinases (MMPs) MMP-2 and MMP-9, and (iii) express selected epithelial–mesenchymal transition markers critical for cell migration and invasion. Administration of luciferase-transfected B16F10-Luc2 melanoma cells resulted in a rapid growth of the tumor and its metastasis to different organs that could be monitored by in vivo bioluminescence imaging as well as by ex vivo BLI of the mouse organs. After tumor cells were administered intravenously in C57Bl/6 mice, administration of cNDs (50 μg i.v. every alternate day) resulted in marked suppression of the tumor growth and metastasis in different organs of mice. Subcutaneous administration of B16F10 cells resulted in robust growth of the primary tumor subcutaneously as well as its metastasis to the lungs, liver, spleen, and kidneys. Intravenous treatment with cNDs did not affect the growth of the primary tumor mass but essentially blocked the metastasis of the tumor to different organs. Histological examination of mouse organs indicated that the administration of cNDs by itself was safe and did not cause toxic changes in mouse organs. These results indicate that the cND treatment may have an antimetastatic effect on the spread of B16F10 melanoma tumor cells in mice. Further exploration of cNDs as a possible antimetastatic therapeutic agent is suggested.

Keywords: carbon nanoparticles, nanodiamonds (ND), carboxyl functionalization, cancer metastasis, cell migration

Significance Statement

Almost 90% of the mortality in cancer is due to tumor metastasis. Any potential therapeutic approach that may inhibit or block the process of metastasis may thus be of great interest clinically. In the present manuscript, we have demonstrated that in vivo treatment of mice administered B16F10 tumor cells (intravenously or subcutaneously) with carboxyl nanodiamonds (cNDs) resulted in an almost complete suppression of tumor metastasis. We suggest that the inhibition of tumor motility and invasiveness may be responsible for the inhibition of the metastatic process. This is a finding not as yet reported in the literature. We think that this finding requires wide dissemination so that the efficacy of cNDs may be explored in other tumor metastasis models and eventually in human patients.

Introduction

Nanodiamonds (NDs) represent a novel category of carbon nanoparticles (CNPs) that are ∼2–8 nm in diameter, though they may agglomerate and form particles of varying sizes (1, 2). The core of NDs comprises sp3 hybridized carbon atoms, while the surface has sp2 hybridized carbon atoms that allow easy functionalization with carboxyl, hydroxyl, and other chemical groups (3). Due to their unique physicochemical properties, and the possibility of easy surface tagging with various chemical groups and drugs, NDs have become an attractive candidate in diagnostics, imaging, and as a therapeutic agent in biomedicine (1, 4, 5). NDs can also be made fluorescent by creating nitrogen vacancy centers in the diamond lattice, and the fluorescence so generated is resistant to photo-bleaching (6). The resulting fluorescent NDs (FNDs) may be used as efficient fluorescent probes for in vitro and in vivo imaging (7).

Functionalization of surface sp2 carbon atoms with negatively charged carboxyl group imparts a negative charge to NDs and renders it more dispersible in aqueous media as well as more interactive with live cells (8, 9). NDs are, in general, biologically inert and do not show significant toxicity in human and animal systems, which make them especially suited for use in biomedical application (10-13). Nontoxicity and biocompatibility of NDs have been demonstrated for 293-T human kidney cells (6); neuroblastoma, alveolar macrophages, and keratinocytes (14); HepG2 and

Competing Interest: The authors declare no competing interest.
Received: March 8, 2023. **Accepted:** October 24, 2023

HeLa cells (15, 16); mouse and human embryonic fibroblast (17); and A549 human lung epithelial cells (18). NDs are well tolerated in nonhuman primates, rats, and by human/rat red blood cells (13, 19, 20) and do not cause significant toxicity when administered in vivo (21, 22).

Our group has been studying the interactions of CNPs like the carbon nanotubes (CNTs) and NDs with biological systems, especially the immune system (23-27). Interestingly, we observed that activated and dividing cells internalize significantly higher amounts of carboxyl CNPs as compared with control resting cells (25). CNPs therefore could be used to target activated cells. A variety of drug molecules may also be attached to the surface of CNPs through the carboxyl group for targeting linked drugs to activated and dividing cells. For in vivo biomedical applications however, NDs are better suited as compared with CNTs, because these are significantly less toxic (20, 28).

Recently, we demonstrated that the carboxyl NDs (cNDs) are efficiently internalized by several epithelial cell lines (29). Epithelial cells treated with cNDs lose their ability to migrate in a scratch wound repair assay as well as across porous membranes in a transwell culture system (29). Considering that in tumor metastasis many steps require the tumor cells to translocate across the tissue extracellular matrix (ECM) as well as across the layer of endothelial cells lining the blood vessels (30, 31), it is possible that the treatment with cNDs may block the metastatic process itself. In the present study, we have explored this proposition by examining the effect of cNDs on the metastasis of B16F10 melanoma cells in mice. Our results clearly demonstrate that the metastasis of the B16F10 melanoma cells was efficiently blocked by the administration of cNDs in tumor-bearing mice. Additionally, the expression of several epithelial–mesenchymal transition (EMT) markers critical for the progression of metastasis was also blocked by the treatment of cNDs in both in vitro and in vivo conditions. Our results may promote further studies to examine the treatment with cNDs as a possible therapeutic approach to counter the process of tumor metastasis.

Materials and methods

Cell culture

The murine melanoma cell line B16F10 (ATCC CRL-6475) and its luciferase transfectant B16F10-Luc2 were kind gifts from Dr. Sanjeev Das (National Institute of Immunology, New Delhi, India). B16F10 cells were cultured under a humidified atmosphere containing 5% CO_2 at 37°C in Dulbecco's modified eagle medium (DMEM) complete medium supplemented with 10% fetal bovine serum, 1% penicillin/streptomycin, and blasticidin (10 μg/ml of media).

Animals and tumor models

Inbred male C57BL/6 mice, 5–12 weeks old (25–35 g body weight), were used throughout the study. Animals were obtained from Rodent Research India, Haryana, and were maintained in the animal house facility at South Asian University, New Delhi. Animals were housed in positive pressure air-conditioned units (25°C, 50% relative humidity) and kept on a 12-h light/dark cycle. Water and chow were provided ad libitum. All the experimental protocols were conducted strictly in compliance with the guidelines notified by the Committee for the Purpose of Control and Supervision on Experiments on Animals (CPCSEA), Ministry of Environment and Forest (https://ccsea.gov.in/WriteReadData/userfiles/file/2006.pdf). The study was duly approved by SAU Institutional Animal Ethics Committee (IAEC project approval code: SAU/IAEC/2016/C.

Two models for studying tumor metastasis were used in the study. For the experimental metastasis model, mice were administered B16F10 or B16F10-Luc2 cells (5×10^5 cells/mouse i.v. in 0.1 ml phosphate-buffered saline [PBS]). From the third day onwards after the tumor cell injection, mice in the cND treatment group received 50 μl suspensions of cNDs containing 50 μg cNDs through i.v. route on every alternate day. For the spontaneous metastasis model, mice were administered B16F10 cells or B16F10-Luc2 cells subcutaneously (1×10^6/mouse in 0.1 ml PBS). Treatment with cNDs as described above was started 10 days after the tumor cell injection.

NDs and other reagents

Both cNDs and carboxylated FNDs (cFNDs) were purchased from Adamas nanotechnology (https://www.adamasnano.com) (Raleigh, USA). cNDs were a colloidal solution of dark gray color that was easily dispersed in water. The average hydrodynamic size and mean zeta potential of the cNDs in aqueous suspension, as determined by the dynamic light scattering characteristics of the particles using the Zetasizer Nano (Malvern Instruments, Malvern, UK), were 43.5 d.nm and −38 meV, respectively. Using a transmission electron microscope (TEM) (model JEOL 2000 FX-II with an ultrathin window fitted with a CCD image recording system) operated at an accelerating voltage of 200 kV, structural examination of NDs was performed. Drop-casting the dispersed samples over the carbon-coated copper grid was employed to perform TEM examination of NDs and cNDs. Because of the functionalized carboxyl group, the reduced aggregation in cND structure is visible in the TEM picture when compared with pristine NDs (Supplementary Fig. S1).

DMEM culture medium and additives were received from HiMedia (Mumbai, India). Transwell 24-well plates (catalog #3422) were purchased from Corning Life Sciences (New York, USA). D-luciferin (catalog no. 88291) was procured from Thermo Fisher (Waltham, MA).

Cellular uptake of NDs

B16F10 cells cultured on a glass cover slip in a 12-well culture plate (0.05×10^6/ml/well) were incubated with cFNDs (10 μg/ml) for 24 h, washed twice with PBS, and fixed with 4% paraformaldehyde. Nuclei were counterstained with Hoechst 33322 dye as described before (25). Cover slips were mounted onto the glass slide with 50% glycerol, and slides were examined on a Nikon A1R Confocal Laser Scanning Microscope (Tokyo, Japan). Using the 3-(4,5-dimethylthiazol-2-yl)-2,5-diphenyltetrazolium bromide (MTT) test, cell viability was examined in vitro. First, cells were grown in 96-well plates at a density of 10^4 cells per well for 24 h and exposed to fresh media containing various cND concentrations for the same period of time. The negative control was cells that just had medium in them. After that, 10 μl of 5 mg/ml MTT dye solution were added to each well and left there for 4 h. Dimethylsulfoxide (DMSO) was used to dissolve Formazan's purple crystals. Cell viability was measured by measuring the reduction of MTT dye optically at 590 nm with the use of a spectrophotometer.

Cell migration and invasion assay

The ability of B16F10 cells to migrate and invade across 8 μm pore size polycarbonate membrane was studied using a 24-well plate transwell system (Corning Life Sciences, NY). Briefly, cells at the density of 3.0×10^4/100 μl/well were cultured in the upper

chamber of the transwell unit in a serum-free medium. The lower chambers of the transwell contained normal culture medium containing 10% fetal bovine serum (FBS) that acted as chemoattractant for cells in the upper chamber. Cells in the upper chamber were treated with cNDs (50 µg/ml), and the transwell setup was incubated at 37°C in a 5% CO_2 atmosphere for 24 h. At the end of the incubation, nonmigrated cells on the upper side of the transwell membrane were gently removed using a cotton swab. Cells that migrated to the lower side of the membrane were fixed with 70% alcohol, stained with crystal violet, and examined under a Nikon phase contrast microscope. The numbers of migrated cells were counted with the help of NIH ImageJ software. Invasion assay was similarly carried out by using Matrigel (catalog no. 354262)-coated membranes in the transwell system (32).

Western blotting

Western blot analyses were performed as previously described with minor modifications (33). B16F10 cells were grown for 24 and 48 h with or without 50 and 100 g/ml cNDs. Cells were washed twice with ice-cold PBS and incubated for 20 min in radioimmunoprecipitation assay (RIPA) lysis solution (Thermo Fisher Scientific, USA) containing a cocktail protease inhibitor mixture (1 µg/ml) and then refrigerated at −80°C overnight. Cell lysates were collected after 24 and 48 h, sonicated three times for 5 s each, and analyzed for protein content using the BCA protein assay kit (Thermo Fisher Scientific). A sample volume of 30 µl (1 µg/µl) of cell lysate proteins was resolved on 8% sodium dodecyl sulfate–polyacrylamide gel electrophoresis (SDS–PAGE) and transferred onto polyvinylidene difluoride (PVDF) membranes (Invitrogen). The transferred membranes were blocked using 5% bovine serum albumin (BSA) for 1 h in Tris-buffered saline with Tween 20 (TBST comprising 25 mm Tris-HCl, pH 7.4, 125 mm NaCl, 0.05% Tween 20). Further, the membranes were probed with the suitable primary antibodies (MMP-2, vimentin, β-catenin, focal adhesion kinase [FAK], fibronectin, E-cadherin, and claudin-1) at recommended dilutions at 4°C for overnight with glyceraldehyde 3-phosphate dehydrogenase (GAPDH) as loading control. Using a horseradish peroxidase (HRP)-conjugated secondary antibodies, the immune complexes were detected by the enhanced chemiluminescence detection system (Bio-Rad).

Gelatin zymography

The levels of MMPs MMP-2 and MMP-9 in the culture supernatant of B16F10 cells were analyzed by gelatin zymography as described elsewhere (27, 34, 35). Briefly, cells (0.5×10^6/ml/well) were cultured in a six-well culture plate in 1 ml complete medium. After 24 h, cells were gently washed with serum-free medium and the culture was continued in the serum-free medium (with or without cNDs, 50 µg/ml) for 24 h. Culture supernatants were collected, centrifuged, mixed with 5X reducing buffer, and subjected to gel electrophoresis using 1% (*w*/*v*) gelatin gel. Following electrophoresis, the gels were incubated with washing buffer (2.5% Triton X-100) with gentle agitation to remove SDS, followed by incubation with incubation buffer (50 mM Tris-HCl buffer, pH 7.4 and 10 mM $CaCl_2$) at 37°C for 24 h to allow digestion of gelatin. The gels were stained with Coomassie Blue solution (0.25 g in 50 ml of staining solution) for 1 h and destained. The white band reveals the gelatinolytic activity zone against the blue background. The bands were scanned and analyzed by NIH ImageJ software.

Histological analysis

Lungs, liver, spleen, heart, and kidneys were harvested, fixed with 4% paraformaldehyde in phosphate buffer, and embedded in paraffin blocks for slicing. Paraffin-embedded 5 µm tissue sections were obtained stained with hematoxylin and eosin (H&E) and analyzed on a microscope (AXIO Zoom V16 microscope).

In vivo bioluminescence imaging

Mice administered with B16F10-Luc2 cells, were anesthetized by intraperitoneal injection of ketamine/xylazine (80 mg of ketamine and 10 mg of xylazine/kg bodyweight) followed by i.p. injection of D-luciferin (150 mg/kg body weight of mouse) 10–15 min before luciferase imaging using the IVIS Lumina II imaging system as described before (36). For ex vivo imaging, animals were administered D-luciferin (150 mg/kg, i.p.) and euthanized after 10 min. Major organs were excised and examined using the IVIS Lumina II imaging system.

Statistical analysis

All experiments were repeated at least three times. Results were expressed in mean ± SD. The paired t test was performed to define the significance of all the experiments. Statistical analyses were performed using SigmaPlot software (Systat Software, San Jose, CA).

Results

In vitro inhibition of cellular motility and invasiveness of B16F10 melanoma cells by cNDs

We have previously demonstrated that for several lung epithelial cell lines, the ability to migrate, both in an in vitro scratch wound repair assay or through a porous membrane in a transwell culture setup, is strongly suppressed by CNTs as well as NDs (29, 37). Since cancer metastasis involves the migration of cancer cells from the primary tumor location to other sites, interference with the ability to migrate may suppress the process of metastasis. The basic question we addressed in this study was whether the CNPs can be used to inhibit the tumor cell migration and therefore the process of metastasis in vivo. cNDs were specifically chosen for this study because of better biocompatibility and lack of toxicity.

To examine the effect of cNDs on the process of metastasis, we used the model of the metastasis of B16F10 melanoma cells in syngenic C57Bl6 mice (38). Results in Figure 1A show that the fluorescent cNDs (cFNDs) are efficiently internalized by B16F10 melanoma cells in culture. The pattern of cFNDs fluorescence inside the B16F10 cells show that the particles are mostly localized in the cytoplasmic areas, though some uptake in the nuclei cannot be ruled out. As observed in our earlier experiments with epithelial cells, migration of B16F10 melanoma cells through transwell membrane was also blocked by treatment with cNDs (Figure 1B and D). Invasiveness of tumor cells was assessed in vitro by their ability to migrate through membranes coated with Matrigel that mimic ECM (32, 39). Results in Figure 1C and D clearly show that while untreated melanoma cells efficiently migrated through the Matrigel-coated membranes (left panel Figure 1C and D), cND treatment reduced it by more than 90% (histogram Figure 1D). Using the MTT cytotoxicity assay, cNDs were found to lack significant toxicity against B16F10 cells (Figure 1E). The potent inhibitory effect of cNDs on cell migration and invasiveness is

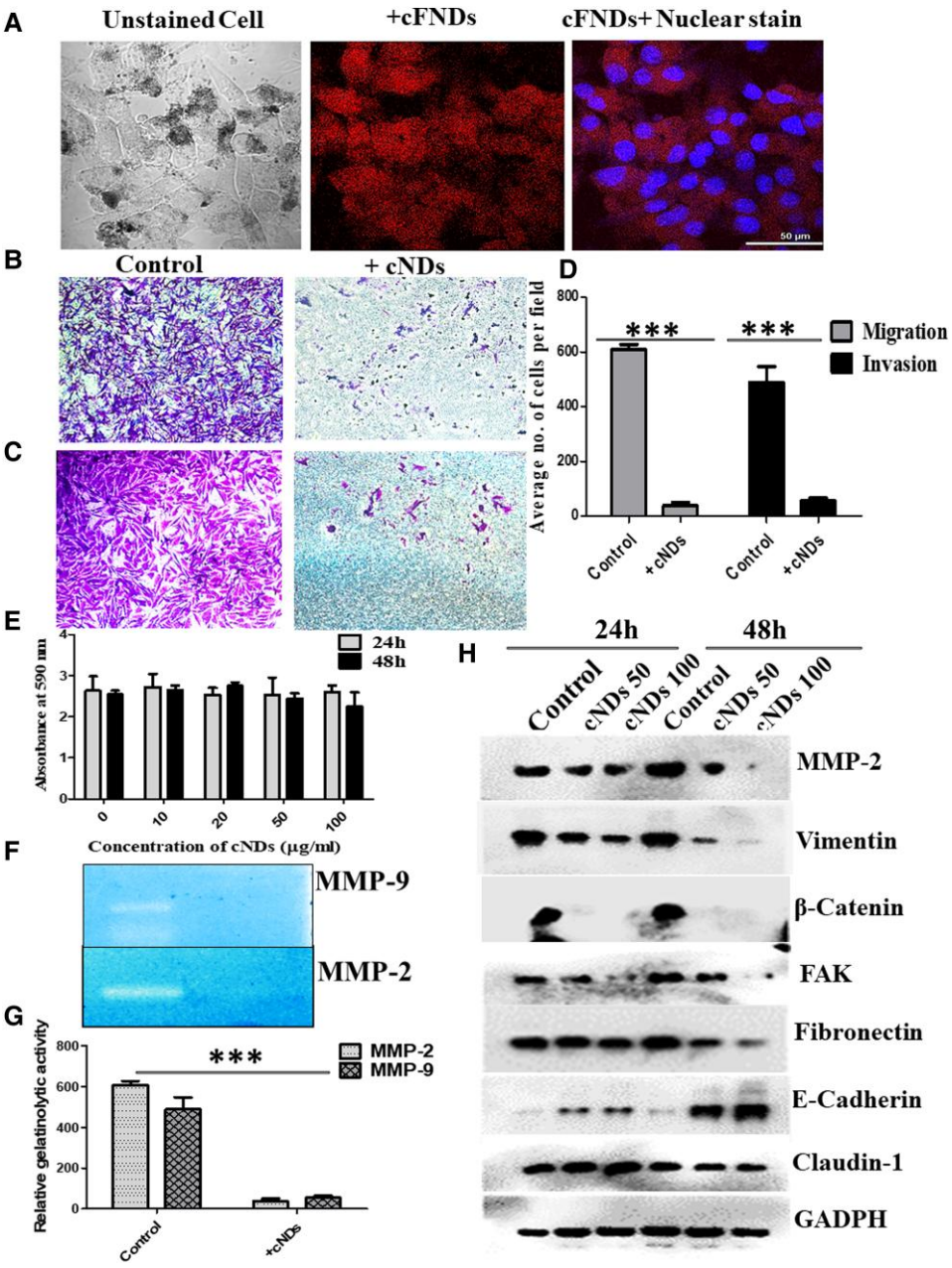

Fig. 1. Uptake of NDs by B16F10 melanoma cells in culture and its effect on cellular migration, invasiveness, viability, secretion of MMPs, and the expression of the EMT markers. A) For cellular uptake of cFNDs, B16F10 melanoma cells (0.05×10^6/ml) were incubated with 10 μg/ml of cFNDs for 24 h. Cells were washed, counterstained with Hoechst 33322 dye as described in the Materials and methods, and examined on a confocal microscope. Fluorescence due to cFNDs, and the nuclear stain are shown. B) Migration of B16F10 cells from the top chamber of the transwell culture system to the bottom of the membrane (with 8 μ pores) separating the top and bottom culture chambers was visualized by staining the cells on the bottom of the membrane as described in the Materials and methods. Normal migration (left of the panel B) and migration in the presence of cNDs (right of panel B) are shown. C) Same as results in panel B except that the membrane separating the top and the bottom culture chambers was precoated with Matrigel. Right panel D shows quantification for the migration and invasion as the means ± SD of number of cells per microscopic view (average of nine view fields). E) B16F10 cells were cultured for 24 or 48 h with or without different concentrations of cNDs, and cell viability was compared by MTT test. F and G) Gelatin zymography results show the release of the MMP enzymes MMP-2 and MMP-9 by control and cND-treated B16F10 cells in culture. Actual gel photographs and quantitative densitometry results are shown. H) Western blotting results of EMT markers in control and cND-treated B16F10 cells after 24 and 48 h of treatment.

not limited to B16F10 cells but is evident in diverse tumor cell types such as 4T1 and MDCK cells (Supplementary Figure S2A, B, and C).

To extrapolate the above in vitro effects of cNDs on B16F10cells to in vivo tumors, it was necessary to demonstrate that the in vivo administered cNDs are efficiently taken up by B16F10 tumors growing in mice. Uptake of cFNDs by B16F10 tumors growing in vivo was examined by using cFNDs. Results in Supplementary Figure S3A show that the cFND particles intravenously administered were efficiently taken up by the tumor mass growing in mouse organs in vivo, indicated by the rich red fluorescence of cFNDs. In tissue sections from control mice as well as tumor-bearing mice without cFNDs treatment, no red fluorescence was detected.

cNDs modulate the expression of EMT markers in B16F10 cells

Since cNDs efficiently blocked cell migration and invasion, crucial steps in tumor metastasis, we next ask whether cNDs modulate the expression of some EMT markers that are known to play a critical role in the regulation of tumor metastasis. First, using the gelatin zymography technique, we found that the secretion of the MMPs MMP-2 and MMP-9, required for invasiveness of tumor cells, was suppressed in cND-treated B16F10 cells (Figure 1F and G). To understand further the underlying mechanism, B16F10 cells with or without cND treatment were examined for the cytosolic expression of some of the important EMT markers such as vimentin, β-catenin, MMP-2, FAK, fibronectin, E-cadherin, and claudin-1. Western blotting results in Figure 1H (after 24 and 48 h treatment with cNDs) show that proteins which are crucial for promoting the EMT process are significantly down-regulated, while major cell adhesion proteins E-cadherin and claudin-1 expression were found to be up-regulated upon exposure to cNDs. The result of both gelatin zymography and Western blotting confirmed the expression of MMP-2 protein which was significantly suppressed in cND-treated cells (Figure 1F, G, and H).

Effect of treatment with cNDs on the growth and metastasis of B16F10 tumor in mice

Bioluminescence imaging (BLI) technique is widely employed in rodent models to assess the progression of tumors in vivo and to evaluate potential therapies (40, 41). In order to assess the progression of B16F10 melanoma tumor growth in mice, luciferase-transfected B16F10 cells (B16F10-Luc2 cells) were used. Growth of luciferase-expressing tumor mass could be visualized in the whole mouse by using the IVIS spectrum system that monitored the luminescence generated within the tumor mass by the luciferase–luciferin reaction.

B16F10-Luc2 cells (5×10^5 cells in 0.1 ml PBS) were administered intravenously, and mice were divided into two groups. The cND treatment group of mice received 50 μg of cNDs on alternate days, while the control group received the vehicle alone. In situ tumor imaging was carried out after 1, 3, and 5 weeks of the administration of the tumor cells. Results of a representative experiment shown in Figure 2 indicate that in the untreated control group of mice, no prominent luminescence signal was detected 1 week postadministration of tumor cells. Significant tumor growth was however detected in this group by the 3-week time point, and it became highly pronounced by week 5. Tumor growth appeared to be mainly confined to the thorax and upper abdominal areas of mice. In the cND-treated group, tumor progression was relatively very low, and only a few minor luminescence spots were observed after 5 weeks (Figure 2A). The presence of tumor growth was also monitored ex vivo in lungs and livers derived from these mice after the 5-week time point. Results in Figure 2B show that the luminescence signal arising from tumor cells was prominent in the lung and liver of untreated control mice but was not detectable in the lung and the livers of cND-treated mice. These results suggest that cND treatment markedly suppressed the appearance of metastatic tumor foci in different organs. Besides a significant decline in tumor metastasis, survival of the tumor-bearing mice treated with cNDs was also significantly better as compared with the survival of untreated tumor-bearing mice (Figure 2C and D).

The above results were further confirmed by directly visualizing the tumor growth in untreated and cND-treated groups of mice. Tumor growth could be visually monitored as the melanoma tumors grew as pitch-black tumor masses. Images of six dissected tumor-administered control mice are shown in Supplementary Figure S4 (panel A). Prominent tumor growths (encircled black tumor masses) were clearly seen in the thorax and abdominal areas of these mice. In marked contrast, in most tumor-administered mice treated with cNDs, no tumor growth was seen (panel B), and even if it occurred, the foci were small and confined to thorax areas.

Gross appearances of the lungs, livers, and spleens derived from the two groups of mice are compared in Figure 3A. Growth of tumors in the lungs of the untreated group of mice is seen as black tumor nodules on the organ surface that were either absent or were highly suppressed in the lungs of cND-treated mice. In livers and lungs, dark black coloration was indicative of melanoma growth in untreated mice that was absent from the livers of the cND-treated mice (Figure 3A). Spleen size in untreated mice was abnormally large (more than double the spleen size in cND-treated mice) due to tumor growth. Quantitative comparisons of the number of metastatic nodules on lung surface and spleen sizes are shown in the histograms in Figure 3B and C, respectively.

Tumor metastasis after directly injecting tumor cells intravenously (experimental metastasis model (42)) involves the extravasation of the injected tumor cells from the blood vessels into the ECM of tissues followed by their migration to new metastasis niches in order to establish metastatic colonies. The above results using the experimental metastasis model suggest that cND treatment may interfere with some step(s) necessary from extravasation of tumor cells, their migration to the metastatic niche, and colonization for successful metastasis.

We further examined the effect of cND treatment in the spontaneous tumor metastasis model that spans the complete metastasis cascade and involves subcutaneous administration of tumor cells in mice (43). B16F10-Luc2 tumor cells were injected subcutaneously (1×10^6 cells/mouse in 0.1 ml PBS), and after 10 days, when the size of the primary tumor growing under the skin was about 1.5 cm, cND treatment (50 μl suspension of cNDs containing 50 μg cNDs through i.v. route on alternate days) was started. After 5 weeks, mice from untreated and cND-treated groups were sacrificed and examined for dissemination of the tumor. Representative results from two mice in each group are shown in Figure 4A and B. These results show that in the untreated mice, there appeared significant metastasis, whereas the cND-treated mice were essentially free of metastasis. Images of the primary tumors excised from the mice are shown under each mouse (Figure 4C and D). It is apparent that the growth of the primary tumors was similar in control and cND-treated mice. Histogram in Figure 4E shows the quantitative data on the comparison of the tumor size in the two groups of mice, and no significant difference was seen between the two sets.

Ex vivo analysis of the tumor foci present in lungs, liver, spleen, and kidneys by BLI is shown in Figure 4F and G. All organs from untreated mice had the luminescence foci indicating the presence of metastasis, whereas the organs from cND-treated mice were free of the metastatic foci. Representative histological data of organs from control and cND-treated mice are given in Figure 4H and I. The presence of black tumor cell is clearly seen in the organs of the untreated mice and not in the organs of the cND-treated mice.

It was necessary to see if the cND treatment by itself was associated with toxicity for the host. Our preliminary data in this regard are shown in Supplementary Figure S5. Administration of cNDs (50 μg/mouse on alternate days for 5 weeks) had no effect on the body weight of the mice (Figure S5A). No difference in the gross appearance (Figure S5B) and the histological pictures of

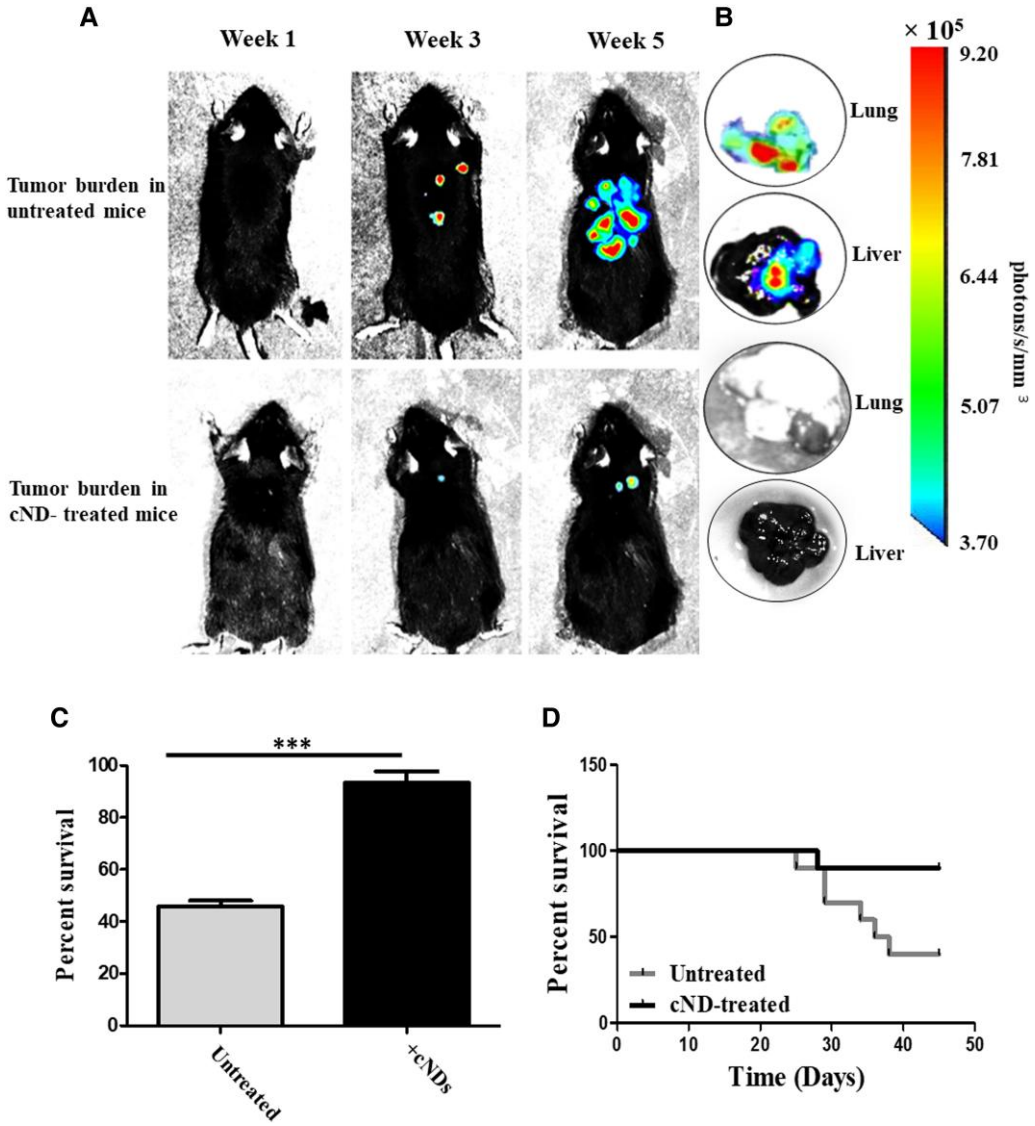

Fig. 2. Effect of treatment with cNDs on the growth and metastasis of B16F10-Luc2 tumor in mice by BLI. C57BL/6 mice were administered B16F10-Luc2 cells (5×10^5/mouse in 0.1 ml of PBS, i.v.). Each mouse in the cND-treated group of mice received 50 µl of cND suspension containing 50 µg cNDs on alternate days for 5 weeks. The mice were imaged at the end of 1, 3, and 5 weeks for the presence of the tumor cells. Ten minutes before the imaging, D-luciferin (150 mg/kg body weight of mouse, i.p.) was administered to generate the bioluminescence signals. A) Relative comparison of BLI images of tumor-bearing mice from the untreated and cNDs treated groups. B) Bioluminescence signals from lungs and livers of the untreated and cND-treated mice showing the presence/absence of tumors. Bioluminescence signal intensity scale is provided on the right of panel B. C) Overall survival percentages for animals in both groups. D) Survival curves of tumor-administered mice in control and cND-treated groups (10 mice per group). Significance of the difference in the two groups, $P < 0.001$.

lungs, livers, spleen, and kidneys could be seen for the two groups of mice (Figure S5C).

Discussion

Tumor cells arise by spontaneous transformation of normal cells in the body. In order to metastasize to distant niches in the body, these primary tumor cells must go through metastasis cascade comprising several distinct steps. These steps include (i) cell proliferation to increase the primary tumor mass and its vascularization to derive nutrition; (ii) breaking away of individual tumor cells from the main tumor mass; (iii) migration of the cells to the nearest blood vessels or the lymph nodes, which requires the cells to be able to move and to exert invasiveness, i.e. the capability to degrade the ECM in order to move; (iv) intravasation of the cells into blood circulation in order to reach new metastasis niches through blood circulation, (v) extravasation of tumor cells from blood vessels, at the site of metastasis; (vi) expression of invasiveness and migratory ability in the extravasated cells in order to reach the metastasis niche; and (vii) proliferation of the cells and vascularization of the metastasized cell mass (44, 45).

Each of these various steps may further require the interplay of a large number of molecules and up-/down-regulation of specific genes, making metastasis an extremely complex process (30, 46). In the spontaneous metastasis animal model, tumor cells instilled subcutaneously would go through all the seven steps described above in order to metastasize. Tumor cells injected intravenously would however require passing through only the last three of these seven steps in order to metastasize. In our present study, we used both subcutaneous and intravenous administration routes to examine the metastasis of B16F10 melanoma cells in various organs like the lungs, liver, spleen, and kidneys. In both models, cND treatment

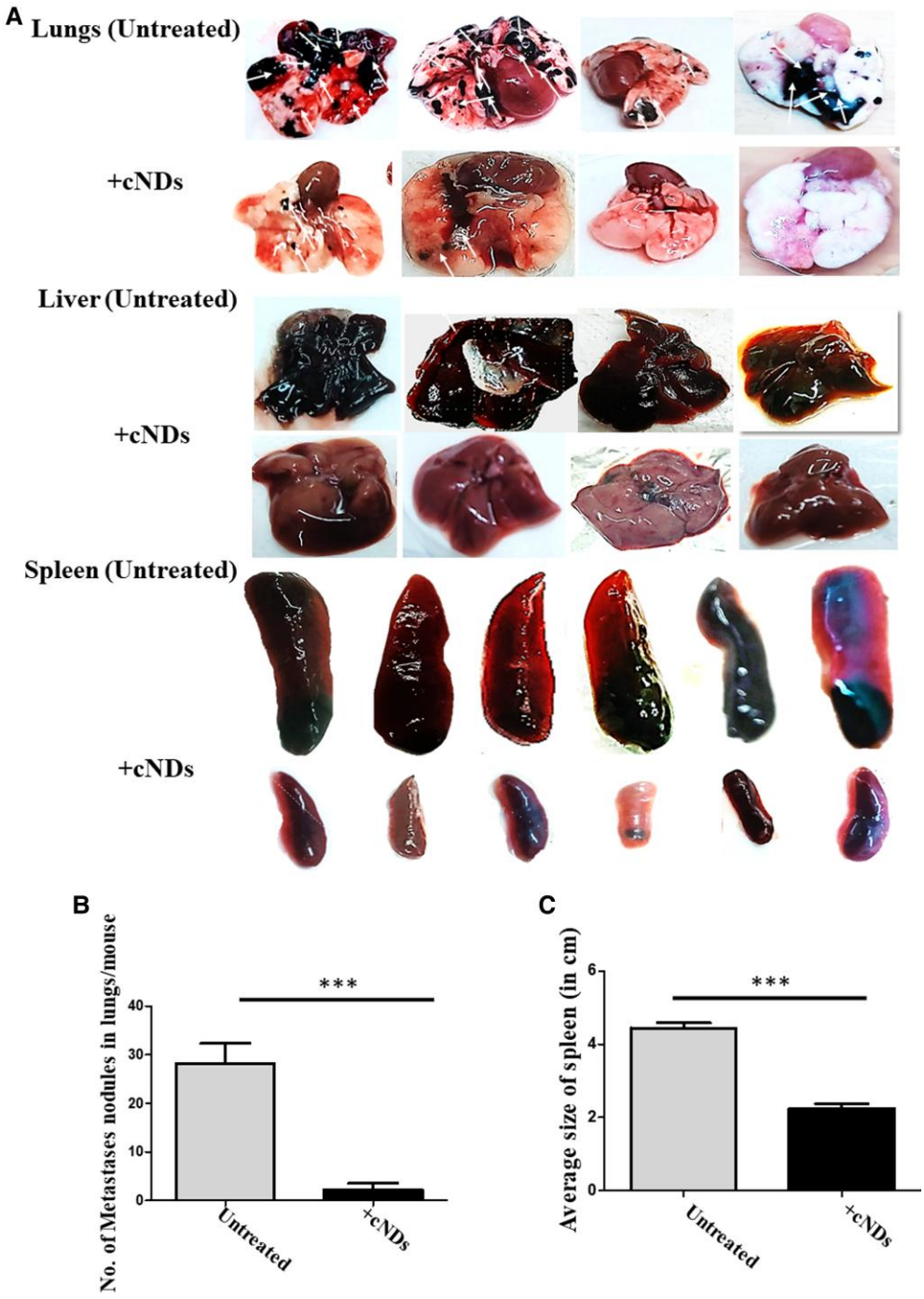

Fig. 3. Direct visualization of growth of tumor foci in mice administered B16F10 tumor cells intravenously and the effect of cND treatment. B16F10-Luc2 tumor cells (5×10^5 cells per mouse/in 0.1 ml of PBS) were injected intravenously into the tail vein of mice. After 2 days, cND treatment (50 μg of cNDs on alternate days for 5 weeks) was started in the cND treatment group of mice. Panel A shows lungs, livers, and spleens isolated from untreated and cND-treated mice at the end of the experiment. White arrows denote the growth of melanoma foci in the lungs. Livers from untreated mice had a black hue due to tumor growth. Spleens from untreated mice were significantly larger in size due to tumor growth, while the spleens from cND treatment group were of normal size. Panel B shows quantitative data of numbers of metastatic nodules on the surface of lungs from untreated and cND-treated mice, and panel C shows the quantitative data on the difference in spleen sizes between the untreated and cND-treated groups of mice (***$P < 0.001$).

strongly suppresses or altogether blocked the tumor metastasis. In order to develop a hypothesis of how cNDs blocked the metastasis, we can consider various steps in the metastasis process listed above and see how cNDs may affect the cellular behavior resulting in the suppression of the metastatic process.

In the spontaneous tumor metastasis model, the first step involves the growth and vascularization of the primary tumor mass. Results in Figure 1G clearly show that cNDs are not toxic to B16F10 cells as there was no decline in the viability of B16F10 cells in the presence of cNDs. Furthermore, the primary tumors grew equally well in both the untreated and the cND-treated mice and attained comparable sizes (Figure 4C, D, and E). It thus appears unlikely that the cNDs interfered with the vascularization of the primary tumor mass or suppressed the cell proliferation in the primary tumor.

In the second step of breaking away of cells from the primary tumor mass, however, our previous results with lung epithelial cell

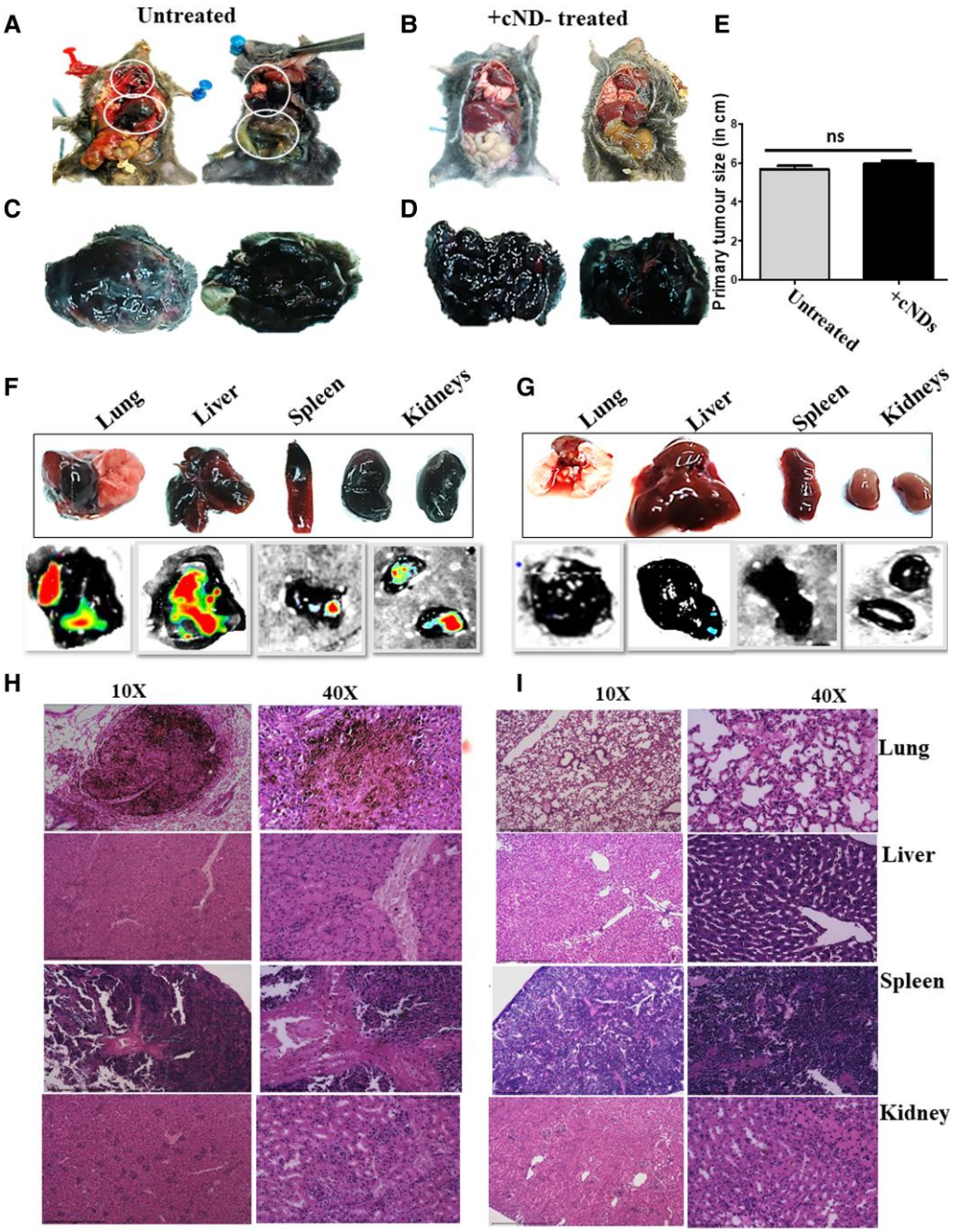

Fig. 4. Growth and metastasis of B16F10 tumors injected subcutaneously in mice and the effect of treatment with cNDs. B16F10-Luc2 cells were administered subcutaneously (1×10^6/mouse/in 0.1 ml of PBS) into the scruff of the neck of mice. Tumors were allowed to grow for 10 days to an average size of 1.5 cm (length-wise) before initiating the cND treatment regimen. Thereafter, the cND treatment group of mice received intravenous cNDs (50 μg on alternate days for 5 weeks). Panels A and B show dissected mice, two each from untreated and cND-treated groups of mice, respectively. Subcutaneous primary tumors isolated from these mice are shown in panels C and D. A quantitative comparison of the sizes of the excised primary tumor from the untreated and the cND-treated groups of mice is shown in panel E, indicating that the size of subcutaneous primary tumor was comparable in the two groups of mice. Ex vivo comparison of the gross appearance of representative lung, liver, spleen, and kidneys from untreated mice and the cND-treated mice and bioluminescence scan images of the organs revealing the growth of tumors are shown in panels F and G. Representative pictures of the histological sections of various organs stained with H&E (at ×10 and ×40 magnifications) are compared in panels H and I.

lines suggest that cNDs could possibly inhibit the breaking away of the cells from the primary tumor mass. This suggestion arises from the fact that the genes that promote migration (β-catenin, vimentin, NM-myosin II, and FAK) were down-regulated in cND-treated epithelial cell lines, whereas the expression of the genes that promote cell-to-cell adhesion (E-cadherin and claudin-1) was not altered (29). While breaking away from the primary tumor mass, tumor cells make a transition from epithelial to mesenchymal phenotype (EMT) and, as a result, display enhanced motile phenotype and invasiveness. These enhanced migration–invasion characteristics are due to the production of ECM degrading gelatinases MMP-2 and MMP-9 and several EMT proteins that aid malignant tumor cells in establishing the tumor progression and metastasis (47). We had previously demonstrated these changes for lung epithelial tumor cell lines like LA4 and A549 cell lines (29, 37). In the current study, we found that the expression

of MMPs and EMT markers such as β-catenin, vimentin, FAK, and fibronectin was significantly suppressed and the expression of epithelial cell adhesion protein E-cadherin and claudin-1 was increased in cND-treated B16F10 cells. Similarly, in tumor-bearing mice, administration of cNDs down-regulated the expression of MMP-2 and β-catenin that otherwise contribute to the invasiveness of tumor metastasis (Supplementary Figure S6A and B). As tumor cells undergoing EMT, a decline in the expression of E-cadherin (epithelial cell-to-cell junction protein) was also observed. This loss in E-cadherin expression is mainly due to the tumor cell mass invasion in the lung parenchymal tissue, whereas in the cND-treated mouse lung, uninterrupted stable junction depicting the expression of E-cadherin was observed (Supplementary Figure S6C). Both the results of in vitro and in vivo tumor samples further validated our proposition that the cND-treated B16F10 tumor cells may tend to stay adhered to each other and not detach/move away from the primary cell mass.

It is in the subsequent four steps in the cascade of metastasis the cNDs may effectively block the process of metastasis. Treatment with cNDs seems to impart a state of immobility in B16F10 cells. We have previously shown that the addition of cNDs blocked cellular migration in a scratch wound repair assay in several epithelial cell lines (29). It is interesting to note that the mobility of the epithelial cells in the scratch wound repair assay is not dependent upon cell proliferation since mitomycin C–treated cells could migrate and fill the wound as efficiently as control cells (Supplementary Figure S7). In addition to our previous results in lung epithelial cells, we have also confirmed that cND treatment efficiently suppressed the migration ability of diverse tumor cell types of different tissue origins such as MDCK (canine kidney cells) and 4T1 (aggressive breast cancer cells) in Supplementary Figure S2. Furthermore, when we recorded the cell migration process for 36 h following a scratch wound in the cell monolayer (live cell imaging video in Supplementary Figure S8), that clearly showed the significant inhibition in cell migration in the presence of cNDs in real-time scenario. Using the B16F10 cells in scratch wound repair assay yielded the same results and blocked the cellular movement in B16F10 cells (our unpublished data). Lacking invasiveness and ability to migrate, cND-treated B16F10 cells may neither be able to reach the afferent lymphatic ducts for entering the regional lymph nodes nor move through the ECM to reach nearby blood vessels; this should seriously compromise the ability of B16F10 cells to metastasize to distant locations. Further, our results in Figure 1 using transwell culture system clearly show that cND-treated B16F10 cells could not traverse membranes with 8 μm pores, in a transwell migration experiment. It is therefore reasonable to assume that cND-treated tumor cells would also be unable to wiggle through the endothelial cell layer that lines the blood vessels. Thus, intravasation of cND-treated tumor cells from tissue matrix into blood vessels and extravasation from blood to ECM may be difficult and may not happen.

In the experimental metastasis model also, where B16F10 cells were directly injected in the blood, cND treatment would take away the ability of these cells in blood circulation to extravasate from the blood vessels and to further move through the ECM to reach the premetastatic niche areas.

Besides the effects discussed above, cNDs could also influence the process of metastasis through other mechanisms. Greten and Grivennikov (48) state that "Inflammation predisposes to the development of cancer and promotes all stages of tumorigenesis" including metastasis. They argue that inflammatory changes in the premetastatic niches prepare and promote the colonization of metastatic foci. We have recently shown that Bacillus Calmette–Guerin (BCG) induced strong inflammatory responses in murine macrophage cell lines RAW264.7 and MHS by up-regulating parameters like production of ROS and nitric oxide and the up-regulation of inflammatory genes like IL1α, IL6, TNFα, iNOS, and Cox-2. Treatment with CNPs like CNTs and the NDs strongly suppressed all these inflammatory responses to BCG treatment (27, 49). It is thus possible that the anti-inflammatory properties of cNDs may also contribute to its overall suppression of the metastatic process. Our own study as well as have shown that many of the inflammatory markers NF-Kb, IL1α, IL6, TNFα, iNOS, and Cox-2 regulate the MMP and EMT marker activation to promote cancer spreading (49–52). Inhibitors of these inflammatory markers and antagonists are known to prevent lung cancer metastasis. cNDs being the effective inhibitors of major inflammatory genes and genes crucial for metastasis could serve as the connecting link and suppress at both the inflammation and tumor metastasis progression levels.

In summary, we have shown in this study that the intravenous administration of cNDs strongly inhibit the metastasis of B16F10 melanoma cells in mice and have presented an argument as to how this inhibitory effect may be exerted at the cellular level. In light of these results, the use of cNDs as a therapeutic agent for cancer metastasis may be further explored.

Acknowledgments

Grant support from the Department of Science and Technology (Nano-Mission) to R.K.S. is gratefully acknowledged. S.P.B. received fellowship support from the Indian Council of Medical Research. The authors acknowledge the kind help of Tarun Sardar for animal work and Nitin Sharma for his help in confocal microscopy. The author would also thank Dr. Narsa Machireddy and Dr. Rizwan Siddique for providing antibodies.

Supplementary Material

Supplementary material is available at *PNAS Nexus* online.

Funding

The study was funded through a research grant to R.K.S. S.P.B. received research fellowship from the Indian Council of Medical Research (ICMR, Govt. of India).

Author Contributions

S.P.B. was a PhD candidate under R.K.S., who is the corresponding author. R.K.S. came up with the idea for this study, which was carried out by S.P.B. with ongoing daily consultations from R.K.S. All laboratory experiments were carried out by S.P.B. under the direction of R.K.S. following consultation with him. Both collaboratively planned the experiments. Additionally, S.P.B. created all the graphs, which were reviewed by R.K.S. The initial draft of the document, which was also written by S.P.B., was reviewed and edited by R.K.S., and the necessary changes were then made. W.T. assisted with the experiment involving BLI and Western blotting.

Data Availability

All the data supporting the findings of this study have been provided within the article and in the supplementary material. Any

additional information required for reanalysis can be obtained upon reasonable request from the corresponding author.

References

1 Mochalin V, Shenderova O, Ho D, Gogotsi Y. 2020. The properties and applications of nanodiamonds. In: Balogh LP, editor. *Nanoenabled medical applications*. Singapore: Jenny Stanford Publishing. p. 313–350.
2 Zhu Y, *et al.* 2012. The biocompatibility of nanodiamonds and their application in drug delivery systems. *Theranostics* 2(3): 302–312.
3 Elugoke SE, *et al.* 2021. Conductive nanodiamond-based detection of neurotransmitters: one decade, few sensors. *ACS Omega*. 6(29):18548–18558.
4 Ansari SA, *et al.* 2016. Role of nanodiamonds in drug delivery and stem cell therapy. *Iran J Biotechnol*. 14(3):130–141.
5 Chauhan S, Jain N, Nagaich U. 2020. Nanodiamonds with powerful ability for drug delivery and biomedical applications: recent updates on in vivo study and patents. *J Pharm Anal*. 10(1):1–12.
6 Yu SJ, Kang MW, Chang HC, Chen KM, Yu YC. 2005. Bright fluorescent nanodiamonds: no photobleaching and low cytotoxicity. *J Am Chem Soc*. 127(50):17604–17605.
7 Alkahtani MH, *et al.* 2018. Fluorescent nanodiamonds: past, present, and future. *Nanophotonics* 7(8):1423–1453.
8 Zheng WW, *et al.* 2009. Organic functionalization of ultradispersed nanodiamond: synthesis and applications. *J Mater Chem*. 19(44):8432–8441.
9 Chang IP, *et al.* 2010. Facile surface functionalization of nanodiamonds. *Langmuir*. 26(5):3685–3689.
10 Schrand AM, Dai L, Schlager JJ, Hussain SM, Osawa E. 2007. Differential biocompatibility of carbon nanotubes and nanodiamonds. *Diam Relat Mater*. 16(12):2118–2123.
11 Paget V, *et al.* 2014. Carboxylated nanodiamonds are neither cytotoxic nor genotoxic on liver, kidney, intestine and lung human cell lines. *Nanotoxicology* 8(sup1):46–56.
12 Moche H, *et al.* 2017. Carboxylated nanodiamonds can be used as negative reference in in vitro nanogenotoxicity studies. *J Appl Toxicol*. 37(8):954–961.
13 Van der Laan K, Hasani M, Zheng T, Schirhagl R. 2018. Nanodiamonds for in vivo applications. *Small* 14(19):1703838.
14 Schrand AM, *et al.* 2007. Are diamond nanoparticles cytotoxic? *J Phys Chem B*. 111(1):2–7.
15 Li J, *et al.* 2010. Nanodiamonds as intracellular transporters of chemotherapeutic drug. *Biomaterials* 31(32):8410–8418.
16 Chen X, Wang H, Li D, Yu Y, Zhi J. 2016. The effect of carboxylated nanodiamond (cNDs) on the migration of HepG2 cells. *physica status solidi (a)*. 213(8):2131–2137.
17 Liu KK, Wang CC, Cheng CL, Chao JI. 2009. Endocytic carboxylated nanodiamond for the labeling and tracking of cell division and differentiation in cancer and stem cells. *Biomaterials* 30(26): 4249–4259.
18 Liu KK, Cheng CL, Chang CC, Chao JI. 2007. Biocompatible and detectable carboxylated nanodiamond on human cell. *Nanotechnology* 18(32):325102.
19 Lin YC, *et al.* 2012. The influence of nanodiamond on the oxygenation states and micro rheological properties of human red blood cells in vitro. *J Biomed Opt*. 17(10):101512.
20 Moore L, *et al.* 2016. Biocompatibility assessment of detonation nanodiamond in non-human primates and rats using histological, hematologic, and urine analysis. *ACS Nano*. 10(8):7385–7400.
21 Puzyr AP, *et al.* 2007. Nanodiamonds with novel properties: a biological study. *Diam Relat Mater*. 16(12):2124–2128.
22 Yuan Y, *et al.* 2010. Pulmonary toxicity and translocation of nanodiamonds in mice. *Diam Relat Mater*. 19(4):291–299.
23 Saxena RK, *et al.* 2007. Enhanced in vitro and in vivo toxicity of poly-dispersed acid-functionalized single-wall carbon nanotubes. *Nanotoxicology* 1(4):291–300.
24 Alam A, Sachar S, Puri N, Saxena RK. 2013. Interactions of polydispersed single-walled carbon nanotubes with T cells resulting in downregulation of allogeneic CTL responses in vitro and in vivo. *Nanotoxicology* 7(8):1351–1360.
25 Dutt TS, Mia MB, Saxena RK. 2019. Elevated internalization and cytotoxicity of polydispersed single-walled carbon nanotubes in activated B cells can be basis for preferential depletion of activated B cells in vivo. *Nanotoxicology* 13(6):849–860.
26 Dutt TS, Saxena RK. 2020. Enhanced antibody response to ovalbumin coupled to poly-dispersed acid functionalized single walled carbon nanotubes. *Immunol Lett*. 217:77–83.
27 Bhardwaj D, Saxena RK. 2021. Poly-dispersed acid-functionalized single-walled carbon nanotubes (AF-SWCNTs) are potent inhibitor of BCG induced inflammatory response in macrophages. *Inflammation* 44(3):908–922.
28 Mohan N, Chen CS, Hsieh HH, Wu YC, Chang HC. 2010. In vivo imaging and toxicity assessments of fluorescent nanodiamonds in *Caenorhabditis elegans*. *Nano Lett*. 10(9):3692–3699.
29 Behera SP, Saxena RK. 2021. Nanodiamonds inhibit scratch-wound repair in lung epithelial cell monolayers by blocking cell migration and inhibiting cell proliferation. *Toxicol Lett*. 341:83–93.
30 Steeg PS. 2016. Targeting metastasis. *Nat Rev Cancer*. 16(4): 201–218.
31 Kai F, Drain AP, Weaver VM. 2019. The extracellular matrix modulates the metastatic journey. *Dev Cell*. 49(3):332–346.
32 Pijuan J, *et al.* 2019. In vitro cell migration, invasion, and adhesion assays: from cell imaging to data analysis. *Front Cell Dev Biol*. 7:107.
33 Singh AP, Mia MB, Saxena RK. 2020. Acid-functionalized single-walled carbon nanotubes alter epithelial tight junctions and enhance paracellular permeability. *J Biosci*. 45:1–12.
34 Yaguchi T, Fukuda Y, Ishizaki M, Yamanaka N. 1998. Immunohistochemical and gelatin zymography studies for matrix metalloproteinases in bleomycin-induced pulmonary fibrosis. *Pathol Int*. 48(12):954–963.
35 Toth M, Sohail A, Fridman R. 2012. Assessment of gelatinases (MMP-2 and MMP-9) by gelatin zymography. *Metastasis Res Protoc*. 878:121–135.
36 Kumari R, Deshmukh RS, Das S. 2019. Caspase-10 inhibits ATP-citrate lyase-mediated metabolic and epigenetic reprogramming to suppress tumorigenesis. *Nat Commun*. 10(1):4255.
37 Behera SP, Saxena RK. 2020. Suppression of in vitro wound healing process in monolayers of lung epithelial cells by poly-dispersed-acid-functionalized-single-walled carbon nanotubes and its mechanism. *Int J Nanotechnol Med Eng*. 5(3):27–41.
38 Bobek V, *et al.* 2010. A clinically relevant, syngeneic model of spontaneous, highly metastatic B16 mouse melanoma. *Anticancer Res*. 30(12):4799–4803.
39 Justus CR, Leffler N, Ruiz-Echevarria M, Yang LV. 2014. In vitro cell migration and invasion assays. *J Vis Exp*. 88:e51046.
40 Jenkins DE, *et al.* 2003. Bioluminescent imaging (BLI) to improve and refine traditional murine models of tumor growth and metastasis. *Clin Exp Metastasis*. 20:733–744.
41 Tiffen JC, Bailey CG, Ng C, Rasko JE, Holst J. 2010. Luciferase expression and bioluminescence does not affect tumor cell growth in vitro or in vivo. *Mol Cancer*. 9(1):1–8.
42 Fowlkes N, *et al.* 2019. Factors affecting growth kinetics and spontaneous metastasis in the B16F10 syngeneic murine melanoma model. *Comp Med*. 69(1):48–54.

43 Khanna C, Hunter K. 2005. Modeling metastasis in vivo. *Carcinogenesis* 26(3):513–523.
44 Welch DR, Hurst DR. 2019. Defining the hallmarks of metastasis. *Cancer Res*. 79(12):3011–3027.
45 Fares J, Fares MY, Khachfe HH, Salhab HA, Fares Y. 2020. Molecular principles of metastasis: a hallmark of cancer revisited. *Signal Transduction Targeted Ther*. 5(1):28.
46 Tahtamouni L, Ahram M, Koblinski J, Rolfo C. 2019. Molecular regulation of cancer cell migration, invasion, and metastasis. *Anal Cell Pathol*. 2019:1–2.
47 Cordani M, Strippoli R, Somoza Á. 2019. Nanomaterials as inhibitors of epithelial mesenchymal transition in cancer treatment. *Cancers (Basel)*. 12(1):25.
48 Greten FR, Grivennikov SI. 2019. Inflammation and cancer: triggers, mechanisms, and consequences. *Immunity* 51(1):27–41.
49 Bhardwaj D, Saxena RK. 2020. Uptake of diamond nanoparticles blocks inflammatory responses in macrophages. *Int J Nanotechnol Med Eng*. 5:4.
50 Hoesel B, Schmid JA. 2013. The complexity of NF-κB signaling in inflammation and cancer. *Mol Cancer*. 12(1):1–15.
51 Huber MA, *et al*. 2004. NF-κB is essential for epithelial-mesenchymal transition and metastasis in a model of breast cancer progression. *J Clin Invest*. 114(4):569–581.
52 Rasmi RR, Sakthivel KM, Guruvayoorappan C. 2020. NF-κB inhibitors in treatment and prevention of lung cancer. *Biomed Pharmacother*. 130:110569.